

# Wavelet Transform-assisted Adaptive Generative Modeling for Colorization

Jin Li, Wanyun Li, Zichen Xu, Yuhao Wang, *Senior Member, IEEE*,  
Qiegen Liu, *Senior Member, IEEE*

**Abstract**—Unsupervised deep learning has recently demonstrated the promise to produce high-quality samples. While it has tremendous potential to promote the image colorization task, the performance is limited owing to the manifold hypothesis in machine learning. This study presents a novel scheme that exploiting the score-based generative model in wavelet domain to address the issue. By taking advantage of the multi-scale and multi-channel representation via wavelet transform, the proposed model learns the priors from stacked wavelet coefficient components, thus learns the image characteristics under coarse and detail frequency spectrums jointly and effectively. Moreover, such a highly flexible generative model without adversarial optimization can execute colorization tasks better under dual consistency terms in wavelet domain, namely data-consistency and structure-consistency. Specifically, in the training phase, a set of multi-channel tensors consisting of wavelet coefficients are used as the input to train the network by denoising score matching. In the test phase, samples are iteratively generated via annealed Langevin dynamics with data and structure consistencies. Experiments demonstrated remarkable improvements of the proposed model on colorization quality, particularly on colorization robustness and diversity.

**Index Terms**—Automatic colorization, Wavelet transform, Unsupervised learning, Generative model, Multi-scale.

## I. INTRODUCTION

Image colorization, the process of adding color to an originally greyscale image, has many practical applications in the computer vision and graphics community [1-3]. As the colorization problem requires a mapping from one-channel grayscale image to multi-channel composite image, it is essentially ill-conditioned and ambiguous with multi-modal uncertainty.

Over the past decades, many approaches including earlier attempts that require user interaction (e.g., scribble-based [4-7] or example-based methods [8-11]) and automatic learning-based methods [12-22], have been developed to tackle the issue of colorization. Among them, traditional methods rely on significant user effort and time to achieve proper results. The supervised methods have the disadvantages of large demand for labeled training datasets and monotonic colorization results. Therefore, some unsupervised learning techniques are heavily investigated in these years. They are remarkably successful in minimizing the use

of training samples and creating diverse colorization results. The most prevailing methods are generative adversarial network (GAN) and variational auto-encoder (VAE). For instance, Yoo *et al.* [13] proposed a model called MemoPainter that can produce high-quality colorization with limited data via GAN and memory networks. Suarez *et al.* [14] used a triplet model based on GAN architecture for learning each color channel independently, in a more homogeneous way. Deshpande *et al.* [12] employed VAE to yield multiple diverse yet realistic colorizations. Recently, some underlying theoretic schemes concerning denoising score matching (DSM) [23], [24] were reported by different research groups. Jayaram *et al.* [25] made a preliminary attempt that treating the colorization task as a color channel separation problem and proposed a “BASIS” separation method based on noise conditional score networks (NCSN) [26] using DSM. NCSN is an iterative generative model where samples are produced progressively via Langevin dynamics using score—the gradients of the data distribution estimated by DSM. Remarkably, it can learn these score functions without adversarial optimization and produce realistic image samples which rival GANs.

Currently, the major deficiencies of score matching based generative models include low data density regions and high dimensional problems in the manifold hypothesis [27], [28]. In fact, there are much previous progressive in improving the naïve NCSN. Quan *et al.* [29] employed the channel-copy technique to form an embedded higher space to enhance score estimation accuracy. Zhou *et al.* [30] learned high-dimensional distribution with score estimation under latent neural Fokker-Planck kernels. In this work, to fully exploit the potential of score estimation to colorization, we leverage the image generation ability embedded with specific wavelet kernel, additionally with constraints in the latent space.

We try to leverage the score-based generative model for colorization by enforcing multi-scale and multi-channel feature aggregation via Discrete Wavelet Transform (DWT). DWT [31-38] is a well-known tool in image processing, which allows images to be decomposed into elementary forms at different positions and scales and subsequently reconstructed with high precision. It has been widely applied in various image processing tasks. For example, Acharya *et al.* [33] proposed an image classification method that processes the input with DWT and demonstrated it can reduce the analyzing time and increase the accuracy. Guo *et al.* [34] suggested training network in wavelet domain to address image superresolution problem as well. There are two key advantages to introduce DWT into this work: One merit is that DWT is a powerful mathematical tool for image processing, which provides an efficient characterization of the coarse and detail frequency spectrums in images. The richer statistics of an image provided in wavelet domain are beneficial for the model to learning prior information than in intensity domain. The other is that DWT provides a mul-

---

This work was supported in part by the National Natural Science Foundation of China under 61871206. J. Li and W. Li are co-first authors. (*Corresponding authors: Yuhao Wang, Qiegen Liu.*)

Jin. Li, Wanyun. Li, Zichen Xu, Yuhao Wang and Qiegen Liu are with the Department of Electronic Information Engineering, Nanchang University, Nanchang 330031, China. ({lijin, liwanyun}@email.ncu.edu.cn, {xuz, wangyuhao, liuqiegen}@ncu.edu.cn)

ti-scale representation of image, which effectively reduces the inherent dimensionality of the data, especially for the high-resolution images with complex patterns. Therefore, it

can reduce the mixing time of Langevin dynamics as well as improving the performance of generative model.

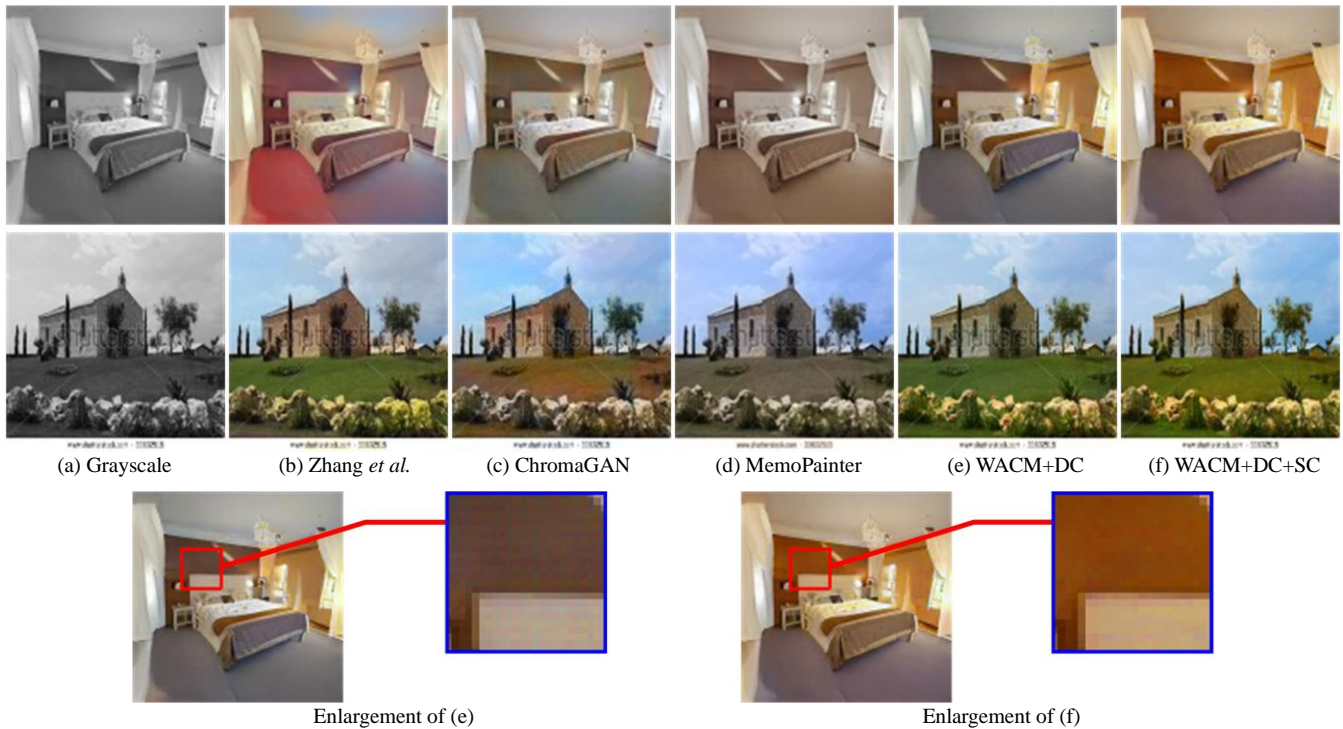


**Fig. 1.** Visual comparison of Zhang *et al.* (b), ChromaGAN (c), MemoPainter (d) and WACM with different constraints (e, f). It can be observed in the first line that Zhang *et al.* (b) assigns unreasonable colors to objects, such as the red floor and blue wall. Meanwhile, the results of ChromaGAN (c) and MemoPainter (d) in the second line suffer from color pollution and desaturation respectively. In this work, dual consistency terms are introduced to leverage the generative model in wavelet domain. The Data-Consistency (DC) in (e) is enforced to achieve a basic proper colorization. Additionally, by enforcing DC and Structure-Consistency (SC) simultaneously, some grid effects shown in (e) can be eliminated to achieve a better colorization image as in (f). The proposed WACM model involved with two consistencies can attain a high-quality colorization performance.

Furthermore, tackling the colorization task in wavelet domain requires some guidance and consistent strategies. As slight deviation of the wavelet coefficients will cause obvious inappropriate effects in the inverse transform result image, post-process is needed to guarantee the transformation relationship between the generated wavelet coefficients. For example, in Fig. 1(e) we can observe the deficiency of the “gridding” effect that appeared in the colorization results. Data-Consistency (DC) and Structure-Consistency (SC) are devised in this study to solve these issues effectively. Among them, DC can guarantee the basic effect of colorization, and SC is used to avoid improper effects and improve the colorization performance. Benefit from the prior learned in multi-scale and multi-channel domain as well as iteratively generate results under the dual consistencies, the proposed Wavelet transform-assisted Adaptive Colorization Model (WACM) performs well in various kinds of image colorization. Comparative experiments against the state-of-the-arts evaluated by qualitative and quantitative metrics demonstrated the superiority of WACM in accuracy, naturalness and diversity.

In summary, the main contributions of this work are as follows:

- **A generative modeling is iterated in wavelet domain:** To alleviate the issue of manifold hypothesis, a novel automatic colorization via score-based generative modeling is used for exploring the prior information in wavelet domain. By stacking the wavelet coefficients as tensors of the network input, prior knowledge learned from multi-scale and multi-channel subspaces jointly paves the way for producing more chances to attain diversity and

possible colorization.

- **Two consistencies are enforced in wavelet domain:** Two consistencies, namely Data-Consistency (DC) and Structure-Consistency (SC) are devised. DC guarantees the basic color performance of the model, and SC is used to reduce inappropriate effects thus improves the colorization performance.

The rest of this paper is presented as follows. Section II briefly describes some relevant works on colorization and 2D-DWT. In section III, we elaborate on the formulation of the proposed method and the dual consistencies. Section IV presents the colorization performance of the present model, including comparisons with the state-of-the-arts, ablation study as well as robustness and diversity test. Discussions and future works are given in Section V and VI, respectively.

## II. RELATED WORK

### A. Image Colorization Techniques

Image colorization refers to estimating the color information from a grayscale image, which provides a practical solution to enhance old pictures as well as expressing artistic creativity. In the past two decades, several colorization techniques have been proposed, ranging from user-guided methods [4-11] to automatic learning-based methods [12-22].

Because of the ill-posed characteristic of colorization, early attempts highly rely on additional user interventions. Considering the amount of user involvement in problem-solving and the way of retrieving the data required, these methods can be roughly categorized into scrib-

ble-based [4-7] and example-based [8-11]. Scribble-based methods generally formulate colorization as a constrained optimization that propagates user-specified color scribbles based on some low-level similarity metrics. Example-based methods focus on coloring the input grayscale image with the color statistics transferred from a reference.

Recently, learning-based approaches have demonstrated their effectiveness in image colorization tasks. Zhang *et al.* [18] considered colorization as a classification task and predicted 313 ‘‘ab’’ pairs of the gamut showing the empirical probability distribution, which were then transformed to ‘‘a’’ and ‘‘b’’ channels of the ‘‘Lab’’ color space. Iizuka *et al.* [19] proposed a deep network with a fusion layer that merges local information dependent on small image patches with global priors computed using the entire image.

Due to the diversity of results and the less reliance on structured datasets, unsupervised learning is considered a promising future direction for image colorization [39]. Cao *et al.* [17] proposed the utilization of conditional GANs for the diverse colorization of real-world objects. They employed five fully convolutional layers with batch normalization and ReLU in the generator of GAN network. Yoo *et al.* [13] proposed a memory-augmented model MemoPainter consists of memory networks and colorization networks to produce colorization with limited data. Zhou *et al.* [16] proposed an iterative generative model which is exploited in multi-color spaces jointly and is enforced with linearly autocorrelative constraint. Victoria *et al.* [15] exploited features via an end-to-end self-supervised generative adversarial network that learns to colorize by incorporating perceptual and semantic understanding.

### B. 2D-DWT

DWT is a well-known tool in image processing community. It is capable of effectively analyzing the image characteristics, especially for image details [32]. Despite wavelets have been applied in many applications such as removing speckle noise from images [35], image classification [36,37], texture analysis [37] and image compression [38], It has seldom applications in image colorization.

The fundamental idea behind DWT is to analyze images according to scale [38], which can produce images at different frequencies. The 2D-DWT is performed by applying the 1D-DWT along the rows and columns separately and subsequently, as shown in Fig. 2(a). The first analysis filter is applied to the row of the image and produces the set of approximate row coefficient and set of details row coefficient. The second analysis filter is applied to the column of the new image and produces four different sub-band images, among which sub-band LL contains approximation information of the original image. The sub-bands denoted HL, LH and HH contain the finest scale detailed wavelet coefficients. Meanwhile, the 2D Inverse DWT (2D-IDWT) traces back the 2D-DWT procedure by inverting the steps, so the components can be assembled back into the original image without losing information [33]. This non-redundant image representation provides better image information compared with other multi-scale representations such as Gaussian and Laplacian pyramids.

Typically, there are various types of wavelets such as Haar [40], Morlet [41], Daubechies [42], etc. Different wavelets may generate various sparse representations of image. In this study, we use the Haar wavelet to linearly decompose the image. As shown in Fig. 2(b), supposing an

$2 \times 2$  image  $I = [[a,b],[c,d]]$ , then the resolution of the four wavelet coefficients is  $1 \times 1$ . The calculation process is as follows:

$$\begin{aligned} cA &= ((a+b)+(c+d))/2 & cH &= ((a+b)-(c+d))/2 \\ cV &= ((a-b)+(c-d))/2 & cD &= ((a-b)-(c-d))/2 \end{aligned} \quad (1)$$

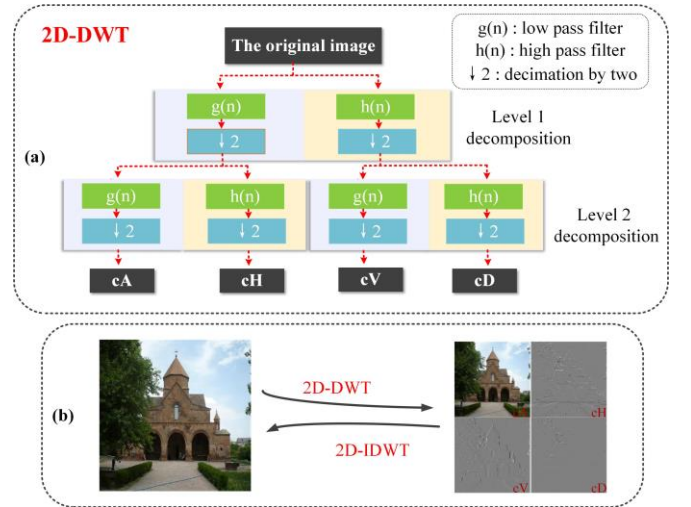


Fig. 2. The procedure of 2D-DWT and 2D-IDWT. (a) The flowchart of 2D-DWT. (b) Example of Haar wavelet.

## III. PROPOSED WACM MODEL

The forward formulation of the colorization task can be mathematically expressed as:

$$y = F(x) \quad (2)$$

where  $y$  and  $x$  denote the gray-level image and the original color image,  $F$  denotes a degenerate function. For example, for a color image in  $RGB$  space, Eq. (2) is often considered as:

$$y = (x_R + x_G + x_B)/3 \quad (3)$$

or

$$y = 0.299x_R + 0.587x_G + 0.114x_B \quad (4)$$

The goal of colorization is to retrieve color information from a grayscale image. As discussed in the related work, generative model has become one of the most important candidates for this task. In this study, the colorization model WACM is iterated in wavelet domain to improve the generative capability of score-based generative model. To further enable accomplish the colorization task and synthesized color to be natural and reasonable, dual consistency terms in wavelet domain are enforced sequentially.

### A. Basic Model: Generation in Wavelet Domain

To advance the colorization task through the generative model with score matching, the first component in WACM is to develop a more sophisticated generation model. Song *et al.* [26] proposed noise conditional score networks (NCSN), which perturbs data with random Gaussian noise to make the data distribution more amenable to score-based generative modeling more precisely. Let  $\{\sigma_i\}_{i=1}^L$  be a positive geometric sequence that satisfies  $\sigma_1/\sigma_2 = \dots = \sigma_{L-1}/\sigma_L > 1$  and  $p_\sigma(\tilde{x}|x) = N(\tilde{x}|x, \sigma^2 \mathbf{I})$ , the unified DSM objective used in NCSN is:

$$L(\theta; \{\sigma_i\}_{i=1}^L) \triangleq \frac{1}{2L} \sum_{i=1}^L \lambda(\sigma_i) E_{p_{data}(x)} E_{p_\sigma(\tilde{x}|x)} \|S_\theta(\tilde{x}, \sigma_i) + (\tilde{x} - x) / \sigma_i^2\|_2^2 \quad (5)$$

where  $\lambda(\sigma_i) > 0$  is a coefficient function depending on  $\sigma_i$ . As a conical combination of DSM objectives,  $S_\theta(x, \sigma)$  minimizes Eq. (6) if and only if  $S_\theta(x, \sigma_i) = \nabla_x \log p_{\sigma_i}(x)$  for all  $i \in \{1, 2, \dots, L\}$ .

After  $S_\theta(x, \sigma_i)$  is determined at the training phase, annealed Langevin dynamics as a sampling approach is introduced. It recursively computes the follows:

$$\begin{aligned} X_{t+1} &= X_t + \frac{\alpha_t}{2} \nabla_x \log p_{\sigma_i}(x_t) + \sqrt{\alpha_t} z_t \\ &= X_t + \frac{\alpha_t}{2} S_\theta(x_t, \sigma_i) + \sqrt{\alpha_t} z_t \end{aligned} \quad (6)$$

where  $\alpha_t$  is the step size by tuning down it gradually.  $t$  is the number of iteration index for each noise level, and  $\forall t: z_t \sim N(0, I)$ .

Although NCSN has achieved good results, its application in data generation is still leaving huge room for improvement, particularly on prior representation and manifold hypothesis. As the foundation of manifold learning, the manifold hypothesis states that certain high-dimensional data with complicated structures can be learned because they lie on or near a much lower-dimensional manifold embedded into the ambient space [43,44]. Block *et al.* [45] proved that in this paradigm, especially for highly structured data such as images, the relevant measure of complexity is the intrinsic dimension of the data rather than any extrinsic features, and the mixing time of the Langevin dynamics used for image generation depends only on this intrinsic dimension. A key conclusion is as follows:

**Theorem 1** (Theorem 1 from [45]). Let  $d \geq 3$  and suppose that the scores of  $p$  and  $p_{\sigma^2}$  are L-Lipschitz and  $(m, b)$ -dissipative. Let  $s_\theta$  be an estimate of the score of  $p_{\sigma^2}$  whose expected squared error with respect to  $p_{\sigma^2}$  is bounded by  $\varepsilon^2$ . Suppose that  $X_0 \sim \nu_0$ . Under technical conditions on  $\nu_0$  satisfied by a multivariate Gaussian, we have

$$\begin{aligned} W_2(\nu_t, p) &\leq (\sigma\sqrt{d} + W_2(\nu_0, p_{\sigma^2})) e^{-\frac{2t}{c_{LS}(p_{\sigma^2})}} \\ &\quad + C\sqrt{(b+d)t}(\varepsilon t + \|p_{\sigma^2}\|_{\infty}^{\frac{1}{2}} e^{\frac{L\sqrt{d}}{4}} \sqrt{t\varepsilon^d})^{\frac{1}{4}} \end{aligned} \quad (7)$$

where  $C$  does not depend on the dimension. As can be seen, the bound of the Wasserstein distance in Eq. (7) is determined by the intrinsic subspace dimension  $d$ . Furthermore, under Assumption 1, the bound will be simpler and more precise.

**Assumption 1.** Let  $(M, g)$  be a  $d'$ -dimensional, smooth, closed, complete, connected Riemannian manifold isometrically embedded in  $\mathbb{R}^d$  and contained in a ball of radius  $\rho$ , such that there exists a  $K \geq 0$  such that  $\text{Ric}_M \geq -Kg$  for all  $y \in M$  in the sense of quadratic forms. With respect to the inherited metric,  $M$  has a volume form  $\text{vol}$ , which has finite total integral on  $M$  due to compactness. Then  $p = p\text{vol}_M$  is continuous with respect to the volume form and we refer to its density with respect to this volume form as  $p$  as well, by abuse of notation.

**Theorem 2** (Theorem 3 from [45]). Suppose that the pair  $(M, g)$  satisfies Assumption 1 and let  $p \propto \text{vol}_M$  be uni-

form on  $M$ . Assume that  $K > 1$  and that  $\kappa > 1$ . Then

$$c_{LS}(p_{\sigma^2}) = O\left(\sigma^2 + K^4 d'^2 \kappa^{20K^2 d'}\right) \quad (8)$$

It should be emphasized that the above bound is completely intrinsic to the geometry of the data manifold and that the dimension of the feature space does not appear, thus we can conclude that even with arbitrarily high dimension in pixel space, if the feasible space has small dimension  $d'$ , Langevin dynamics will still mix quickly.

Following the above theoretical derivation, the authors in [45] proposed a multi-resolution strategy based on upsampling to reduce the intrinsic dimension of the data, which can effectively transfer some of the hard work of score estimation to the easier, lower-dimensional regime, as well as boosting the performance of generative model. This way falls into the progressive strategy; It generates image from low-dimensional resolution to high-dimensional resolution progressively. Unfortunately, compared with the naïve NCSN, the numerical experiments demonstrated that the progressive strategy to utilizing the multi-resolution scheme lacked significant improvement.

Our idea is also motivated by the manifold hypothesis and the theoretical analysis above. By contrast, in this work we present a substantially different way to achieve the goal. By means of wavelet transform, NCSN learns and iterates in wavelet domain to improve the prior learning ability and generation effect. Different from the “sequence” method in [45], we take advantage of the multi-scale feature of wavelet transform in a “joint” manner by decomposing the image into less amount of low-frequency information with the complex structured correlation between coordinates and more amount of relatively simple high-frequency information, thus to reduce the intrinsic dimension in wavelet domain. Furthermore, owing to representing the image as wavelet coefficients, the generative model can learn richer priors in the wavelet domain than in intensity domain. In addition, beneficial with the IDWT process, the generated wavelet coefficients can be assembled back into the reference image with high accuracy at the sampling stage, which will not lose information or take extra time.

In details, supposing  $x$  is a target image containing the three color-channel of  $R, G, B$ , it can be expressed as  $x = [x_R, x_G, x_B]$ . Applying DWT to each channel, it yields

$$\begin{aligned} W(x_R) &= [cA_R, cH_R, cV_R, cD_R] = W_R \\ W(x_G) &= [cA_G, cH_G, cV_G, cD_G] = W_G \\ W(x_B) &= [cA_B, cH_B, cV_B, cD_B] = W_B \end{aligned} \quad (9)$$

where  $W_R, W_G$  and  $W_B$  are three four-channel tensors superimposed by the four sub-band images whose resolution is one-quarter of the reference.

Stacking the three tensors together, a 12-channel tensor  $X = [W_R, W_G, W_B]$  is obtained to train the network. The goal of stacking to be  $X$  is to form object in multiple lower-dimensional manifold jointly that in favor of the subsequent network learning [29], [48], thus avoiding potential difficulties for both accuracy in score estimation and sampling with Langevin dynamics. Accordingly, the objective of WACM is:

$$L(\theta; \{\sigma_i\}_{i=1}^L) = \frac{1}{2L} \sum_{i=1}^L E_{p_{\text{data}}(x)} E_{p_{\sigma_i}(\tilde{x}|X)} \lambda(\sigma_i) \left\| S_\theta(\tilde{X}, \sigma_i) + (\tilde{X} - X) / \sigma_i \right\|_2^2 \quad (10)$$

To investigate the multi-scale and joint-learning strategy of WACM, we train the naïve NCSN and WACM on CelebA

dataset in  $64 \times 64$  and  $128 \times 128$ , respectively. The intermediate generated results of modeling in wavelet domain are shown in Fig. 3. It can be observed that, as the iteration increases, the intermediate results approach the ground truth gradually. The low-frequency component mixes at an earlier stage (i.e., the fifth column), meanwhile, the other high-frequency components mix more slowly (i.e., the seventh column).

The generation comparison between the results of modeling in intensity and wavelet domain is shown in Fig. 4. The generation effect of WACM is significantly better than the naïve NCSN for CelebA  $128 \times 128$ . In addition, because the face position of the CelebA data set is aligned and the face images are relatively smooth. The data distribution of the high-frequency wavelet coefficients is relatively regular and the network can learn the prior and generate the subspace

information faithfully.

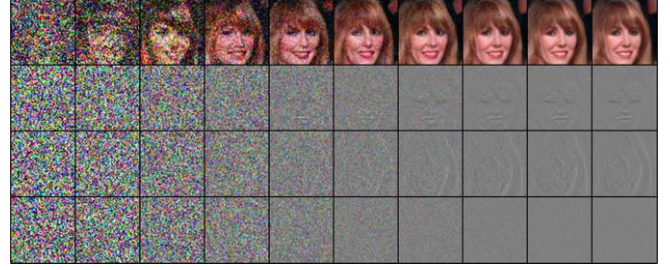


**Fig. 3.** Sampling trajectories of the wavelet coefficients. Notice that the low-frequency component mixes at an earlier stage (i.e., the fifth column), at the same time, the other high-frequency components mix more slowly (i.e., the seventh column).

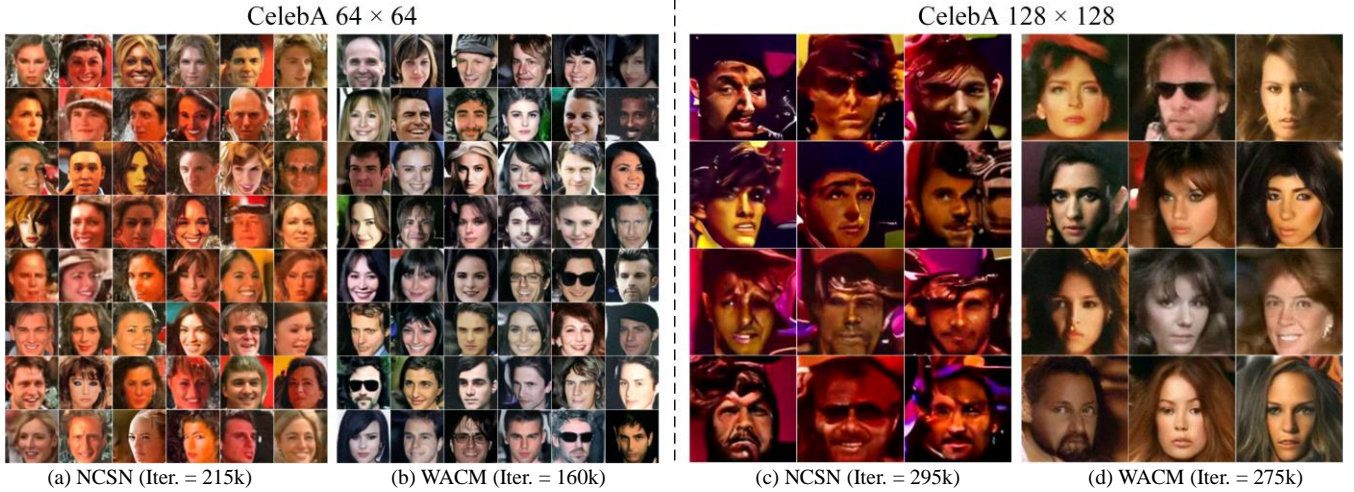


**Fig. 4.** The visual results generated by the model of naïve NCSN in intensity domain and WACM in wavelet domain. Left:  $64 \times 64$ , right:  $128 \times 128$ . It can be observed that naïve NCSN performs fair against our model in  $64 \times 64$  images. Both of them generate appropriate and realistic results in (a)(b). However, influenced by the curse of dimension, naïve NCSN is not capable to generate complete and clear results in higher resolution images with size of  $128 \times 128$  and only generates chaos images with basic features of human faces as the results illustrated in (c). By contrast, benefited from the multi-scale strategy, our results perform excellently in  $128 \times 128$  images. Especially, our model performs significantly better than naïve NCSN. This phenomenon strongly indicates the superiority and effectiveness of this strategy.

### B. Colorization Model: Two Consistencies in WACM

The key to utilize score-based generative model for colorization and reduce the intrinsic limitation lies in the design of proper consistency strategies. Consequently, in the second component of WACM, data-consistency and structure-consistency are devised to guide the model to achieve superior colorization performance.

1) **Data-Consistency in Wavelet Domain:** To limit the uncertainty of the generative model and guide it to colorize on the input grayscale image, a data-consistency term (DC) is proposed and added in the iterative procedure. More precisely, the DC term guides the generative model to complete the colorization task on the input grayscale by minimizing the error between the observed value of the intermediate result at each iteration and the sub-band image of the original input.

Because of the linear relationship between the degenerate function  $F$  and the Haar wavelet  $W$ , the order of the two operations is commutative. Thus, the following equation can be obtained as:

$$W(y) = W(F(x)) = F(W(x)) \quad (11)$$

and

$$\begin{aligned} cA_y &= F(cA_R, cA_G, cA_B) & cH_y &= F(cH_R, cH_G, cH_B) \\ cV_y &= F(cV_R, cV_G, cV_B) & cD_y &= F(cD_R, cD_G, cD_B) \end{aligned} \quad (12)$$

Therefore, the DC term can be directly applied to the

wavelet domain, that is, the 12 channels of  $X$  as:

$$DC(X) = \lambda \|F(W(x)) - F(y)\| = \lambda \|F(X) - W(y)\| \quad (13)$$

where  $\lambda$  is a hyper-parameter that is related to the noise level at the current iteration.

The colorization results of WACM with only data-consistency in wavelet domain are shown in Fig. 5. It illustrates that, after the DC term is enforced, the model already can perform basic colorization on the input grayscale image, but due to the deviation of the generated wavelet coefficients, the final effect still has certain structural defects.

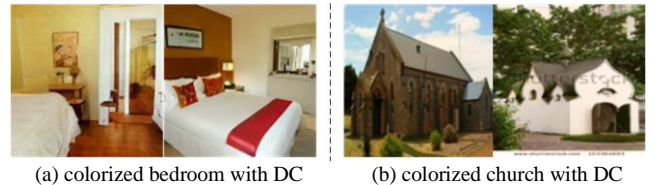


**Fig. 5.** Results generated by WACM with DC term. Although the colorization results are natural overall, it suffers from improper grid effects in detail.

2) **Structure-Consistency in Wavelet Domain:** The proposal of the Structure-Consistency (SC) is based on the observation of the overall RGB color deviation and grid phenomenon in the colorization results after the DC term is applied.

As shown in Fig. 6, we respectively output the histograms

of the high-frequency wavelet coefficients of the  $R$ ,  $G$ , and  $B$  channels of the original color picture and the gridded picture. It can be noticed that due to the inherent freedom of the generative model, the data distribution of the obtained  $cH$ ,  $cV$ , and  $cD$  have certain deviations compared with the original  $RGB$  image. Since the IDWT result is very sensitive to the wavelet coefficients, especially the high frequency components, these deviations will cause display defects of edge differences and grid phenomenon in the final colorization results.

Considering the characteristics of the data distribution and value range of the wavelet coefficients in DWT, the mean value of the wavelet coefficients of the grayscale can be regarded as approximately equal to the mean value of the wavelet coefficients of the original color image. Thus, we devise the SC term. For the  $i$ -th channel  $X_i$  in  $X$ , SC can be expressed as:

$$SC(X_i) = Mean(X_i) - Mean(W(y_i)) \quad (14)$$

For each channel of  $X$ , the SC is the difference between the mean value of the channel and the mean value of the corresponding wavelet coefficient of the input grayscale image. The calculated SC of each channel is a real number and  $X$  is modified by subtracting the difference from each pixel value of the corresponding channel.

After each iteration, SC is used to correct the iteration results, and shift the values of wavelet coefficients as a whole to make it satisfy the transform and inverse transform relationship. Notably, the SC term will inevitably lead to certain side effects. For example, due to the difference between the intensity of the  $RGB$  channel of the original color image and the grayscale, applying SC to the low-frequency wavelet coefficients of some images will result in the saturation of the final colorization effect lower than the unconstrained circumstance.

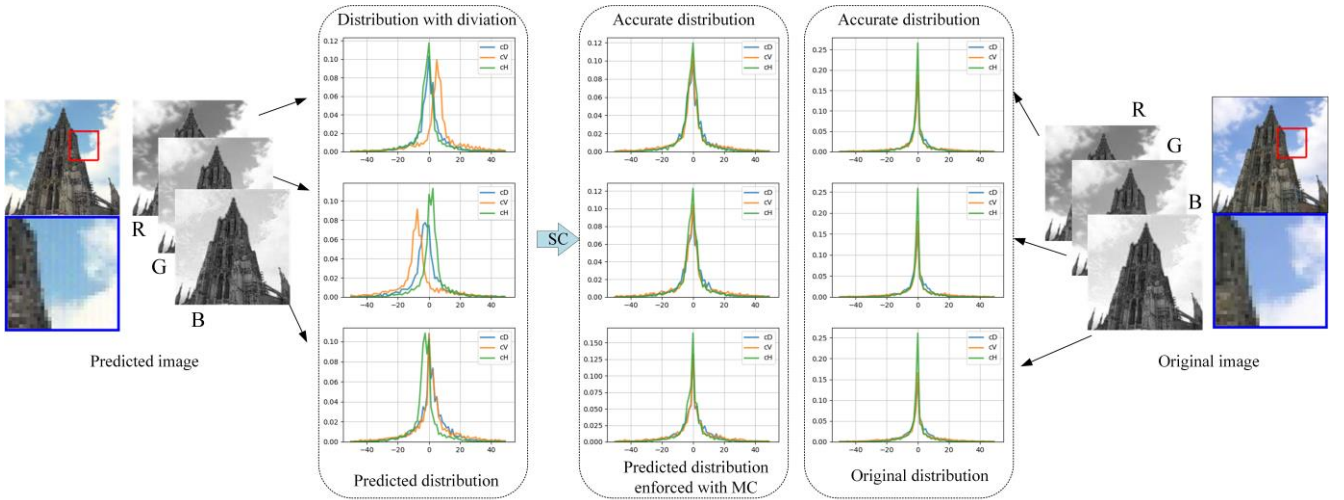


**Fig. 6.** The histograms of the high-frequency wavelet coefficients of the  $R$ ,  $G$ , and  $B$  channels of the original image (a) and the predicted image (b). Compared with the original image, the high-frequency histograms of the generative image have dissimilar distributions, which leads to errors in the edge and "gridding" effects of the generated image.

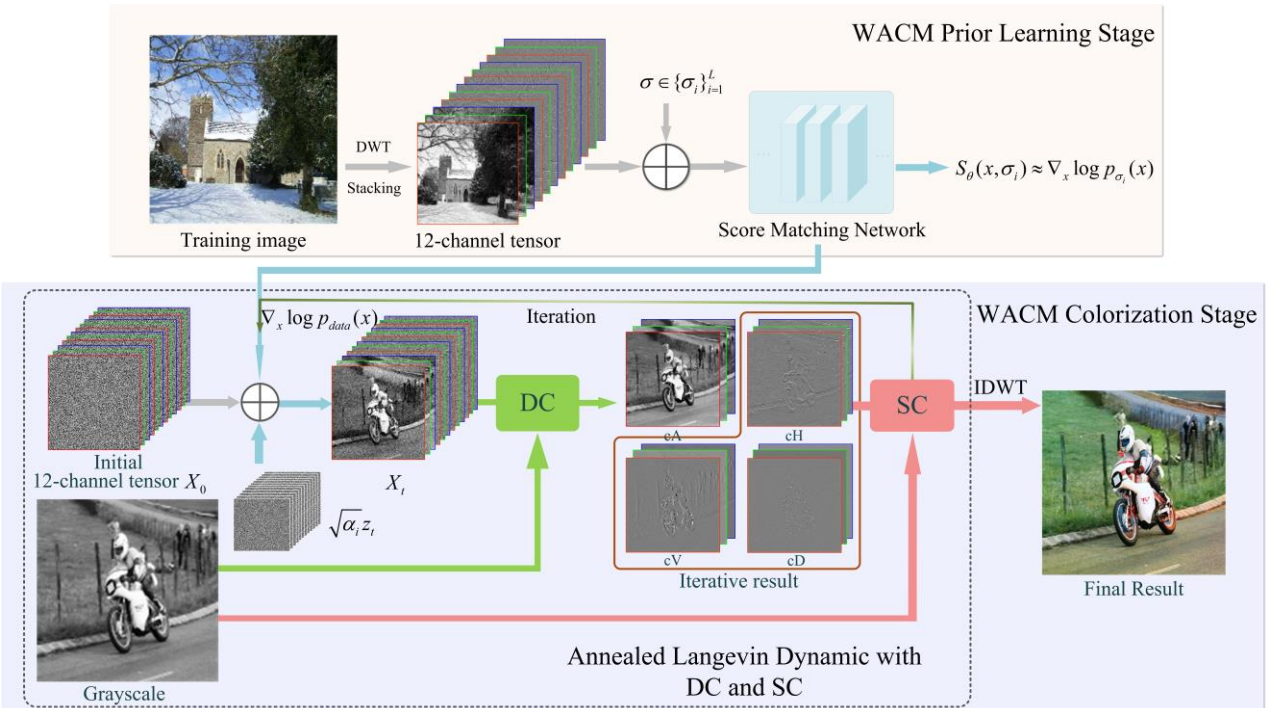


**Fig. 7.** Iterative colorization procedure of WACM. Specifically, in the prior learning stage, the network  $s_\theta(x)$  learns to retrieve  $\nabla_x \log p_{data}(X)$  in wavelet domain that best matches the ground truth of the input image. In the colorization stage, WACM generates samples from the 12-dimensional noisy data distribution by annealed Langevin dynamics with data-consistency. At the meantime, the structure-consistency is used to improve the performance and reduce the improper effects of the samples. Here symbol “ $\oplus$ ” stands for the sum operator, “DC” and “SC” stands for data-consistency and structure-consistency.

### C. Summary of WACM

With the above-mentioned dual consistency terms, the model can better utilize the wavelet transform in the colorization task with score matching. Overall, as Fig. 7, the entire colorization diagram includes two processes: learning prior information in wavelet domain and iterative generate colorization process.

Specifically, in the training phase, a set of 12-channel tensors are formed by applying wavelet transform to the  $R$ ,  $G$ ,  $B$  channels of an image respectively to train the DSM network in the multiple low-dimensional space. After the network is trained, the model can sample with the annealed Langevin dynamics which recursively computes the following formula which is modified with the data-consistency term:

$$X_{t+1} = X_t + \frac{\alpha_t}{2} s_\theta(X_t, \sigma_t) - \lambda DC(X_t) + \sqrt{\alpha_t} z_t \quad (15)$$

where  $\forall t: z_t \sim N(0, I)$ .

In the sampling process, a 12-channel tensor  $X_0$  is initialized from the uniform noise as input of the first iteration. Then generate a list of noise levels  $\{\sigma_i\}_{i=1}^L$  that are reduced proportionally for each step of the outer loop. At each iteration, run Langevin dynamics to sample intermediate result from  $p_{\sigma_i}(X)$  and added artificial noise to it according to the noise level  $\sigma_i$ . The transition helps smoothly transfer the benefits of large noise levels to low noise levels where the perturbed data are almost indistinguishable from the original one. In the meantime, the data consistency is incorporated into the update of iterative generative process, forming the iterative reconstruction procedure. Finally, at  $\sigma_L \approx 0$ ,  $p_{\sigma_L}(X)$  is close to  $p_{data}(X)$  and the results of color channels expressed in wavelet coefficients are obtained.

After the sampling process is completed, the proposed structure-consistency is performed to the generated wavelet coefficients. Finally, the final result can be attained by performing an inverse wavelet transform on the iteratively generated wavelet coefficients. The whole sampling process is explained in **Algorithm 1**.

---

#### Algorithm 1 Iterative Colorization via WACM

---

● **Initialization:**

- (a) Set parameters  $\varepsilon, L, T$ , and  $\beta$ .
- (b) Initialize noise level  $\{\sigma_i\}_{i=1}^L$  and  $X_0 \sim U(-1, 1)$ .

● **Outer loop:** for  $i = 1, 2, \dots, L$  **do**

- (a) Set the step size  $\alpha_i = \varepsilon \cdot \sigma_i^2 / \sigma_L^2$ .
- (b) **Inner loop:** for  $t = 1, 2, \dots, T$  **do**

$$X_{t+1} = X_t + \frac{\alpha_t}{2} s_\theta(X_t, \sigma_t) - \lambda DC(X_t) + \sqrt{\alpha_t} z_t.$$

**End for**

- (c) Calculate  $SC(X_T)$  via Eq. (12).
- (d) Update  $X_T = X_T - \beta SC(X_T)$ .
- (e) Output the colorization result  $x = IDWT(X_T)$ .

**End for**

---

## IV. EXPERIMENTS

In this section, after the experimental setup is detailed, the present WACM is compared with the state-of-the-arts qualitatively and quantitatively. Then, several key factors that contribute to the final WACM are separately investigated.

Finally, two main advantages of WACM are exhibited: colorization robustness and diversity. For the purpose of replicate research, the code is available at: <https://github.com/yqx7150/WACM>.

### A. Experiment Setup

1) **Datasets:** We experiment with multiple image datasets from various sources as follows:

LSUN [49] (bedroom and church): LSUN contains around one million labeled images for each of 10 scene categories and 20 object categories, including bedroom, fixed room, living room, classroom, church, and so on. In this study, we choose the indoor scene LSUN-bedroom dataset and the outdoor scene LSUN-church dataset to validate the robustness of WACM.

COCO-stuff [50]: The COCO-stuff is a subset of the COCO dataset [51] generated for scene parsing. It contains 164k images that span over 172 categories, including 80 things, 91 stuff, and 1 class unlabeled, most of which are natural scenes with various objects.

2) **Implementation Details:** The proposed WACM selects the UNet-type architectures with instance normalization and dilated convolutions as the network structure. Adam is chosen as an optimizer with a learning rate of 0.005 and halved every 5,000 iterations. Subsequently, at the training phase, we reshape each image into  $128 \times 128$  pixels and  $256 \times 256$  pixels as preprocessing, the WACM model is trained for 500,000 iterations in each dataset with a batch size of 8 that takes around 40 hours. The model is performed with Pytorch interface on 2 NVIDIA Titan XP GPUs, 12 GB RAM. At the testing stage, we randomly choose 100 images from the validation set for each dataset, then 12 results are produced for each grayscale image to test our model.

3) **Evaluation Metrics:** Two quantitative assessments of our method are included in terms of peak signal to noise ratio (PSNR) and structural similarity index measure (SSIM). In brief, denoting  $x$  and  $\hat{x}$  to be the colorized image and ground-truth, the PSNR is defined as:

$$PSNR(x, \hat{x}) = 20 \log_{10} \text{Max}(\hat{x}) / \|x - \hat{x}\|_2 \quad (16)$$

and the SSIM is defined as:

$$SSIM(x, \hat{x}) = \frac{(2\mu_x \mu_{\hat{x}} + c_1)(2\sigma_{x\hat{x}} + c_2)}{(\mu_x^2 + \mu_{\hat{x}}^2 + c_1)(\sigma_x^2 + \sigma_{\hat{x}}^2 + c_2)} \quad (17)$$

Besides, to evaluate the realism of the colorized image, a user study is designed to qualitatively evaluate the methods as well.

### B. Comparisons with State-of-the-arts

To demonstrate the superiority of the proposed WACM, we compare it with four state-of-the-art colorization methods quantitatively and qualitatively, including Zhang *et al.* [18], MemoPainter [14], ChromaGAN [15] and iGM [16].

1) **Quantitative Metrics:** In this experiment, we randomly select 100 images from LSUN-bedroom, LSUN-church, and COCO-stuff datasets, respectively, and resize them to be  $128 \times 128$ , then calculate the average PSNR and SSIM values of the results that colorized by different methods. Table 1 and Fig. 8 summarize the colorization performance of WACM and other state-of-the-art methods on  $128 \times 128$  images.

One can observe that, in general, the PSNR and SSIM values of WACM are higher than most of those obtained by other methods. In LSUN-church dataset, WACM achieves the highest PSNR and SSIM values, as well as the highest

PSNR values in LSUN-bedroom dataset. For COCO-suff dataset which consists of more complex outdoor images, the ability of generative model is limited to a certain extent. WACM still represent strong colorization performance with the help of the multi-scale and multi-channel strategies, and the value of PSNR is slightly lower than that of ChromaGAN.

TABLE I

COLORIZATION COMPARISON OF OUR SYSTEM TO STATE-OF-THE-ART TECH-

NIQUES IN THE 128×128 IMAGES.

| Algorithm           | LSUN-church  | LSUN-bedroom | COCO-stuff   |
|---------------------|--------------|--------------|--------------|
| Zhang <i>et al.</i> | 23.65/0.9228 | 20.89/0.8946 | 20.21/0.8844 |
| MemoPainter         | 21.66/0.8767 | 22.92/0.8975 | 22.05/0.8929 |
| ChromaGAN           | 24.63/0.9106 | 24.16/0.8899 | 22.98/0.8924 |
| iGM-6C              | 20.60/0.8953 | 22.40/0.9099 | 19.68/0.8493 |
| WACM                | 25.44/0.9265 | 24.13/0.9056 | 22.41/0.8810 |



Fig. 8. Visual comparisons with the state-of-the-art on images with the size of 128×128. From left to right: Grayscale, Ground truth, Zhang *et al.*, ChromaGAN, MemoPainter, iGM and two diversity results of WACM. The present WACM can predict more visually pleasing colors.

For the sake of comparison, some results are depicted in Fig. 8. Overall, the results of other methods provide sometimes vivid colors as in the second line and sixth line in Fig. 8(d) and sometimes uncolored results as in the sixth line in Fig. 8(c)(e). However, their results suffer from the issues of color pollution and desaturation. On the contrary, WACM yields better results in terms of consistent hue, saturation, and contrast, etc. For example, in the third row of Fig. 8(g), there are no discordant green colors on the ground like (c) and (d), and the image of WACM in the second row has obvious contrast in luminance between table lamp and the bed. The quantitative comparison to state-of-the-art methods indicates the superiority of WACM in aspects of naturalness and structural characteristics, including luminance, contrast, and structure.

Furthermore, to prove the contribution of wavelet transforms to the colorization performance of higher resolution images. Two diversity colorization results of WACM on 256×256 images are shown in Fig. 9. It can be appreciated that the results of the proposed WACM are quite realistic and diverse. The results further illustrate the superiority of

WACM in promoting colorization task on higher resolution images by integrating multi-scale and multi-channel strategies with score-based generative model.

2) *User Study*: Similar to [52], we utilize the Two-Alternative Forced Choice (2AFC) paradigm to design user study. We choose five random colorized results generated by four methods (ChromaGAN, MemoPainter, Zhang *et al.* and WACM) to make the comparison and invite 68 users in different age groups to participate in this user study. For each target image, there are 6 pairs of colorized results to make sure any two methods are compared. The order of image pairs is randomized to avoid bias.

During the experiment, the users are asked to choose one of each pair that looks more natural. The total number of user preferences (clicks) for each colorization result is recorded, which is shown in Fig. 10. The highest total clicks imply that the colorization of the proposed method is mostly preferred by users. Besides, the lowest standard deviation indicates that colorization results of WACM are always satisfactory despite different image content.





**Fig. 9.** Some colorization results of WACM in  $256 \times 256$  resolution. The image in the first row is the input grayscale, and the images in the second and third rows are two diverse results of WACM. Benefit from the multi-scale and multi-channel characteristics of DWT, WACM produces high-quality colorization results in higher resolution images, which alleviates the difficulty of NCSN to generate high-resolution images.

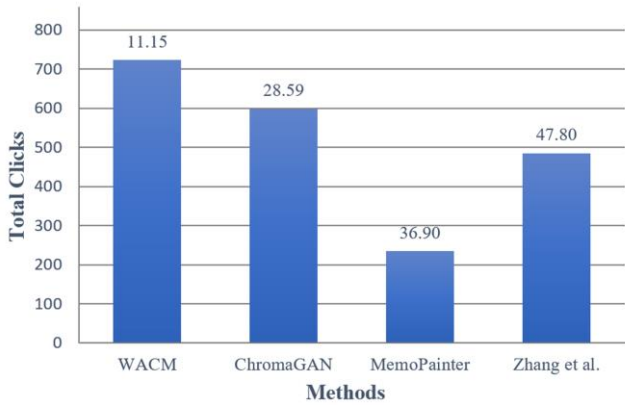


**Fig. 10.** The total value and standard deviation (shown above the bar) of user clicks for five colorization results obtained by different methods.

### C. Ablation Study

Three main components are critical to the performance of the final WACM: prior learning in wavelet domain, training high-frequency and low-frequency wavelet coefficients jointly, and structure-consistency that enforced in wavelet domain. Here several ablation studies are conducted to validate these important designs.

1) **Prior Learning in Wavelet or Intensity Domain:** We conduct an experiment to quantify the key factor of this research—training DSM in wavelet domain. Previously, Jayaram *et al.* [25] had proposed a “BASIS” separation method based on the naive NCSN in intensity domain and made a preliminary attempt on colorization task by treating it as a color channel separation problem. We report the quantitative comparisons of prior learning in wavelet domain and intensity domain on LSUN-church and LSUN-bedroom datasets in Table 2 and exhibit two examples in Fig. 11. The results present a significant performance boost gained by our method in all metrics, which further highlights the contribution of prior learning in wavelet domain. The significant improvement of SSIM is worth noting, for example, increase by 0.8 in LSUN-church dataset, and 0.9 in LSUN-bedroom

dataset, which is benefited by the complete description of details and texture of the image at all available scales via DWT.

TABLE II  
QUANTITATIVE COMPARISONS FOR ABLATION STUDY OF PRIOR LEARNING IN DIFFERENT DOMAINS ON LSUN-CHURCH AND LSUN-BEDROOM DATASETS.

| Domain           | LSUN-church         | LSUN-bedroom        |
|------------------|---------------------|---------------------|
| Intensity domain | 22.67/0.8584        | 20.29/0.8150        |
| Wavelet domain   | <b>25.44/0.9265</b> | <b>24.13/0.9056</b> |

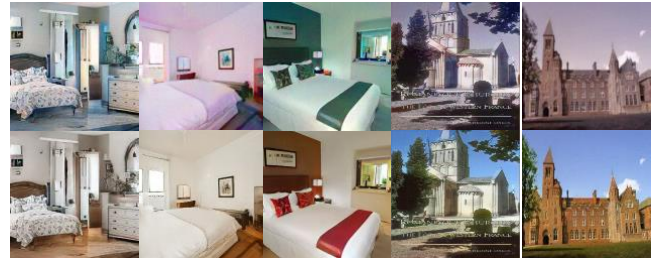


**Fig. 11.** Quantitative and qualitative comparisons between prior learning in intensity domain (the first line) and wavelet domain (the second line).

2) **Training Wavelet Coefficients Jointly or Separately:** In this experiment, we investigate the colorization performance on two settings: joint training or separate training of high-frequency and low-frequency wavelet coefficients, namely WACM-joint and WACM-divide. The quantitative comparisons are conducted on LSUN-church dataset to evaluate their performance. Fig. 12 and Table 3 list the comparison results. Generally, thanks to the multi-scale prior information, both of them can produce satisfactory results. However, results in Table 3 present a performance boost gained by WACM-joint.

An important reason for the superior performance of joint training is that training separately cannot guarantee the consistency of the high-frequency and low-frequency wavelet coefficients generated by the network. Another possible reason is sampling in the high-dimensional embedding space is more effective than the information obtained from

low-dimensional objects [48]. In addition, a single network can effectively reduce the amount of computation cost thus improves the efficiency of the model.

TABLE III  
COLORIZATION COMPARISON OF WACM-JOINT AND WACM-DIVIDE IN THE 128×128-PIXEL IMAGE OF LSUN-CHURCH DATASET.

| Algorithms  | PSNR  | SSIM   |
|-------------|-------|--------|
| WACM-joint  | 25.44 | 0.9265 |
| WACM-divide | 22.71 | 0.9023 |

3) *Iteration with Different Consistencies*: This ablation study is conducted to investigate the contribution of SC in wavelet domain. WACM is sampling under two different cases: without/with SC term. Fig. 13 provides qualitative and quantitative comparisons. As shown, although the former results accomplish the correct colorization and have a high saturation overall, they suffer from improper gridding effects in details, which causes the colorization results cannot achieve higher PSNR or SSIM values and have imperfect visual effects.

However, the later model with SC can constrain the generation of high-frequency wavelet coefficients and guide it toward the correct distribution, thus effectively eliminates the “gridding” artifacts. We also zoom in on the partial map for



Fig. 13. Quantitative and qualitative comparisons between (a) WACM only with DC and (b) WACM with both DC and SC. The comparison results in (a)(b) validate a performance boost gained by using SC. It can be noticed that both the PSNR and SSIM improved under the constraint of SC as well as eliminating the “gridding” artifacts visually. This experiment demonstrated that SC helps to achieve finer results.

#### D. Robustness Test

Due to the wide application of colorization task but the datasets in real-world may insufficient, it is impossible to train the model with all types of images. Therefore, the robustness of model, i.e., one model for tackling various images in different datasets, is necessary.

Considering natural images contain the potential priors of multiple types of pictures, in this section, we use a model only trained by COCO-stuff to handle a variety of colorization tasks, including legacy black-and-white photos and cartoons.

1) *Colorizing Legacy Black-and-White Photos*: Different from colorizing the pictures from the test datasets, which processes the original color images to obtain the grayscale images and then colorize them. In more general cases, we can only observe the grayscale image  $y$  without knowing its forward model  $F$ . In this circumstance, the task of “blind” colorization is more challenging.

In this experiment, a prevailing processing method of forming  $F$  is chosen:

$$F(x) = (x_R + x_G + x_B) / 3.0 \quad (18)$$

observation. It can be observed that the results in Fig. 13(b) retains the merits of high saturation and proper color but reduces the improper edge effects appearing in Fig. 13(a). The results attain a performance boost gained by using SC, especially in terms of SSIM value, which is a metric as to structural characteristics. This experiment demonstrates that SC operation indeed helps to achieve finer results.



Fig. 12. Colorization comparison of the proposed WACM between separate training and joint training of high-frequency and low-frequency wavelet coefficients. Top line: WACM-joint, Bottom line: WACM-divide.

As observed in Fig. 14, convincing results are generated by WACM. Taking the second picture for example, the results are realistic in terms of texture, contrast and saturation.

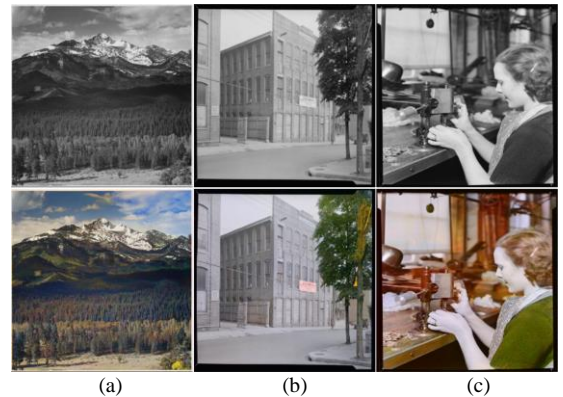
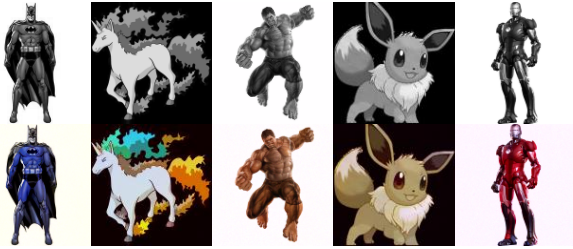


Fig. 14. Colorizing legacy black and white photographs. Our model can obtain realistic colorization results whether it is a picture of landscapes or close-ups. The images we choose are (a) Colorado National Park, 1941 (b) Textile Mill, June 1937 (c) Hamilton, 1936.

2) *Colorizing Cartoons*: When it comes to real-world ap-

plications, cartoons and animation are two main areas needed for colorization. However, data for animations and cartoons are often limited as the cartoon images are difficult to create and must intricately be colored by hand. This problem can be alleviated by training the model in natural image datasets that have abundant images and then applying it to cartoon colorization.

In this experiment, we try to learn wavelet prior from the COCO-stuff dataset and apply it to colorize cartoons, some results of WACM are exhibited in Fig. 15. Although the accuracy of manual colorization cannot be achieved, the results produced by WACM are satisfactory and quite good. As can be seen in the second image, the cartoon characters are colored in blue and orange and obtained color consistency. In the fifth image, the textures of the character (the metallic texture of the character body) are retained as well.



**Fig. 15.** Colorize cartoon images. The top line involves the observed grayscale image. The bottom line lists the result obtained by WACM. Notice that all these results are obtained automatically by WACM without model re-training in the cartoon dataset.

In most cases, WACM can produce realistic and satisfactory results. Notably, in all tests, WACM is only trained in the COCO-stuff dataset. This phenomenon indicates the effectiveness and robustness of WACM.

### E. Colorization Diversity

Image colorization is essentially a one-to-many task as multiple feasible colorized results can be given for the same grayscale input. Generating a diverse set of colorization solutions is an effective way to tackle this multi-modality challenge. In general, it can be achieved via generative models.

Leveraging the generative model as well as multi-scale and multi-channel prior learning, our model can generate multiple feasible colorized images to meet different needs. Some diverse colorization results are shown in Fig. 16. The results demonstrate our generated colored images have fine-grained and vibrant colors and look realistic.



**Fig. 16.** Illustration of the diverse colorization by WACM. For each image, WACM produces twelve colorized samples, four different styles are chosen. It can be noticed that WACM can produce various styles for a single image.

## V. CONCLUSIONS

To summarize, this work proposed an iterative generative model in wavelet domain to address the colorization problem. We have shown that utilizing the multi-scale and multi-channel strategies to make the prior learning procedure in lower-dimensional subspace via wavelet transform is an effective optimization scheme to improve the performance of score-based generative models. By taking advantage of the non-redundant and multi-scale representation of DWT and the high-precision reconstruction of IDWT, we can address some general problems in the unsupervised model. Meanwhile, two consistency terms are proposed to make full use of wavelet coefficients while avoiding the improper effects caused by the uncertainty of generative model. Extensive experiments were conducted to demonstrate that the proposed method achieved state-of-the-art performance in automatic colorization, and showed strong superiority over the previous methods in both quantitative and qualitative assessments.

## REFERENCES

- [1] A. Fatima, W. Hussain, and S. Rasool, "Grey is the new RGB: How good is GAN-based image colorization for image compression," *Multimed. Tools Appl.*, vol. 80, no. 3, pp. 3775-3791, 2021.
- [2] M. H. Baig and L. Torresani, "Multiple hypothesis colorization and its application to image compression," *Comput. Vis. Image Underst.*, pp. 111-123, 2017.
- [3] Y. Bian, Y. Jiang, Y. Huang, X. Yang, W. Deng, H. Shen, R. Shen, and C. Kuang, "Deep learning virtual colorization overcoming chromatic aberrations in singlet lens microscopy," *APL Photonics*, vol. 60, no. 3, 2021.
- [4] A. Levin, D. Lischinski, and Y. Weiss, "Colorization using optimization," *ACM Trans. Graph.*, vol. 23, no. 3, pp. 689-694, 2004.
- [5] Y. Huang, Y. Tung, J. Chen, S. Wang, and J. Wu, "An adaptive edge detection based colorization algorithm and its applications," *ACM Multimedia*, 2005, 1, 2.
- [6] Y. Qu, T. T. Wong, and P. A. Heng, "Manga colorization," *ACM Trans. Graph.*, vol. 25, no.3, pp. 1214-1220, 2006.
- [7] Q. Luan, F. Wen, D. Cohen-Or, L. Liang, Y. Xu, and H. Shum, "Natural image colorization," *Proceedings of the 18th Eurographics conference on Rendering Techniques*, pp. 309-320, 2007.
- [8] T. Welsh, M. Ashikhmin, and K. Mueller, "Transferring color to greyscale images," *Proceedings of the 29th annual conference on Computer graphics and interactive techniques*, vol. 21, no. 3, 2002.
- [9] R. Ironi, D. Cohen-Or, and D. Lischinski, "Colorization by example," *Proceedings of the Eurographics Symposium on Rendering Techniques*, pp. 201-210, 2005.
- [10] G. Charpiat, M. Hofmann, and B. Scholkopf, "Automatic image colorization via multimodal predictions," *European conference on computer vision*, pp. 126-139, 2008.
- [11] A. Y. S. Chia, S. Zhuo, R. K. Gupta, Y. Tai, S. Cho, P. Tan, and S. Lin, "Semantic colorization with internet images," *ACM Trans. Graph.*, vol. 30, no. 6, pp. 1-8, 2011.
- [12] A. Deshpande, J. Rock, and D. Forsyth, "Learning large-scale automatic image colorization," *Proceedings of the IEEE International Conference on Computer Vision*, pp. 567-575, 2015.
- [13] S. Yoo, H. Bahng, S. Chung, J. Lee, J. Chang, and J. Choo, "Coloring with limited data: Few-shot colorization via memory augmented networks," *Proc. IEEE Conf. Comput. Vis. Pattern Recognit.*, pp. 11283-11292, 2019.
- [14] P. L. Suárez, A. D. Sappa, and B. X. Vintimilla, "Infrared image colorization based on a triplet dcgan architecture," *IEEE/CVF Conf. on Comp. Vision and Pattern Rec.*, pp. 18-23, 2017.
- [15] P. Victoria, L. Raad, and C. Ballester, "ChromaGAN: adversarial image colorization with semantic class distribution," *Proceedings of the IEEE/CVF Winter Conference on Applications of Computer Vision*, pp. 2445-2454, 2020.
- [16] J. Zhou, K. Hong, T. Deng, Y. Wang, and Q. Liu, "Progressive colorization via iterative generative models," *IEEE Signal Process. Letters*, vol. 27, pp. 2054-2058, 2020.
- [17] Y. Cao, Z. Zhou, W. Zhang, Y. Yu, "Unsupervised diverse colorization via generative adversarial networks," *Machine Learning and Knowledge Discovery in Databases*, vol. 10534, Springer, Cham, pp. 151-166, 2017

- [18] R. Zhang, P. Isola, and A. A. Efros, "Colorful image colorization," *Proc. Euro Conf. Comput. Vis.*, pp. 649-666, 2016.
- [19] S. Iizuka, E. Simo-Serra, and H. Ishikawa, "Let there be color! joint end-to-end learning of global and local image priors for automatic image colorization with simultaneous classification," *ACM Trans. Graph.*, vol. 35, no. 4, pp. 1-11, 2016.
- [20] P. Isola, J.-Y. Zhu, T. Zhou, and A. A. Efros, "Image-to-image translation with conditional adversarial networks," *IEEE/CVF Conf. on Comp. Vision and Pattern Rec.*, pp. 1125-1134, 2017.
- [21] A. Deshpande, J. Lu, M. C. Yeh, M. J. Chong, and D. Forsyth, "Learning diverse image colorization," *IEEE/CVF Conf. on Comp. Vision and Pattern Rec.*, pp. 6837-6845, 2017.
- [22] J. Zhao, J. Han, L. Shao, and C. G. Snoek, "Pixelated semantic colorization," *Int. J. Comput. Vision*, pp. 1-17, 2019.
- [23] P. Vincent, H. Larochelle, Y. Bengio, and P.A. Manzagol, "Extracting and composing robust features with denoising autoencoders," *Proc. Int. Conf. Learn. Represent.*, pp. 1096-1103, 2008.
- [24] P. Vincent, "A connection between score matching and denoising autoencoders," *Neural Comput.*, vol. 23, no. 7, pp. 1661-1674, 2011.
- [25] V. Jayaram and J. Thickstun, "Source separation with deep generative priors," *International Conference on Machine Learning*, pp. 4724-4735, 2020.
- [26] Y. Song and S. Ermon, "Generative modeling by estimating gradients of the data distribution," *Proc. Adv. Neural Inf. Process. Syst.*, pp. 11895-11907, 2019.
- [27] H. Narayanan and S. Mitter, "Sample complexity of testing the manifold hypothesis," *Proc. Adv. Neural Inf. Process. Syst.*, vol. 2, pp. 1786-1794, 2010.
- [28] S. Rifai, Y. N. Dauphin, P. Vincent, Y. Bengio, and X. Muller, "The manifold tangent classifier," *Proc. Adv. Neural Inf. Process. Syst.*, vol. 24, pp. 2294-2302, 2011.
- [29] C. Quan, J. Zhou, Y. Zhu, Y. Chen, S. Wang, D. Liang, and Q. Liu, "Homotopic gradients of generative density priors for MR image reconstruction," *IEEE Trans. Med. Imag.*, 2021.
- [30] Y. Zhou, C. Chen, and J. Xu, "Learning high-dimensional distributions with latent neural Fokker-Planck kernels," *arXiv preprint arXiv:2105.04538*, 2021.
- [31] A. N. Akansu, P. A. Haddad, R. A. Haddad, and P. R. Haddad, "Multiresolution signal decomposition: transforms, subbands, and wavelets," *Academic Press*, 2001.
- [32] D. Zhang, "Wavelet transform", *Fundamentals of Image Data Mining*, pp. 35-44, 2019.
- [33] M. Acharya, S. Poddar, A. Chakrabarti, and H. Rahaman, "Image Classification Based on Approximate Wavelet Transform and Transfer Learning on Deep Convolutional Neural Networks," *International Symposium on Devices, Circuits and Systems*, pp. 1-6, 2020.
- [34] T. Guo, H. Seyed Mousavi, T. Huu Vu, and V. Monga, "Deep wavelet prediction for image super-resolution," *IEEE/CVF Conf. on Comp. Vision and Pattern Rec.*, pp. 104-113, 2017.
- [35] A. Sharma, A. Khunteta, "Satellite image contrast and resolution enhancement using discrete wavelet transform and singular value decomposition," *International Conference on Emerging Trends in Electrical Electronics & Sustainable Energy Systems*, pp. 374-378, 2016.
- [36] K. H. Ghazali, M. F. Mansor, M. M. Mustafa, A. Hussain, "Feature extraction technique using discrete wavelet transform for image classification," *5th Student Conference on Research and Development*, pp. 1-4, 2007.
- [37] C. Zhu, X. Yang, "Study of remote sensing image texture analysis and classification using wavelet," *Int. J. Remote Sens.*, vol. 19, no. 16, pp. 3197-3203, 1998.
- [38] M. M. H. Chowdhury and A. Khatun, "Image Compression Using Discrete Wavelet Transform," *International Journal of Computer Science Issues*, vol. 9, no. 4, pp. 327, 2012.
- [39] S. Anwar, M. Tahir, C. Li, A. Mian, F. S. Khan, and A. W. Muzaffar, "Image colorization: A survey and dataset," *arXiv preprint arXiv:2008.10774*, 2020.
- [40] R. S. Stanković and B. J. Falkowski, "The Haar wavelet transform: its status and achievements," *Computers & Electrical Engineering*, vol. 29, no. 1, pp. 24-44, 2003.
- [41] J. Lin and L. Qu, "Feature extraction based on Morlet wavelet and its application for mechanical fault diagnosis," *J. Sound Vib.*, vol. 234, no. 1, pp. 135-148, 2000.
- [42] C. Vonesch, T. Blu, and M. Unser, "Generalized Daubechies wavelet families," *IEEE Trans. Signal Process.*, vol. 55, no. 9, pp. 4415-4429, 2007.
- [43] C. Fefferman, S. Mitter, and H. Narayanan, "Testing the manifold hypothesis," *J. Am. Math. Soc.*, 29, February 2016. doi: 10.1090/jams/852.
- [44] M. Belkin and P. Niyogi, "Laplacian eigenmaps for dimensionality reduction and data representation," *Neural Comput.*, vol. 15, no. 6, pp. 1373-1396, 2003.
- [45] A. Block, Y. Mroueh, A. Rakhlin, J. Ross, "Fast mixing of multi-scale Langevin dynamics under the manifold hypothesis," *arXiv preprint arXiv:2006.11166*, 2020.
- [46] P. Baldi, "Autoencoders, unsupervised learning, and deep architectures," *ICML workshop on unsupervised and transfer learning, JMLR Workshop and Conference Proceedings*, pp. 37-49, 2012.
- [47] D. P. Kingma and M. Welling, "Auto-encoding variational bayes," *International Conference on Learning Representations*, 2014.
- [48] Q. Liu, Q. Yang, H. Cheng, S. Wang, M. Zhang, and D. Liang, "Highly undersampled magnetic resonance imaging reconstruction using autoencoding priors," *Magn. Reson. Med.*, vol. 83, no. 1, pp. 322-336, 2020.
- [49] F. Yu, A. Seff, Y. Zhang, S. Song, T. Funkhouser, and J. Xiao, "LSUN: Construction of a large-scale image dataset using deep learning with humans in the loop," *arXiv preprint, arXiv:1506.03365*, 2015.
- [50] H. Caesar, J. Uijlings, and V. Ferrari, "Coco-stuff: Thing and stuff classes in context," *Proc. IEEE Conf. Comput. Vis. Pattern Recognit.*, pp. 1209-1218, 2018.
- [51] T. Y. Lin, M. Maire, S. Belongie, J. Hays, P. Perona, D. Ramanan, ..., and C. L. Zitnick, "Microsoft coco: Common objects in context," *European conference on computer vision*, pp. 740-755, 2014.
- [52] F. Fang, T. Wang, T. Zeng, and G. Zhang, "A superpixel-based variational model for image colorization," *IEEE Trans. Visual Comput. GR.*, vol. 26, no. 10, pp. 2931-2943, 2019.